

Possible shape coexistence and magnetic dipole transitions in  $^{17}\text{C}$  and  $^{21}\text{Ne}$ H. Sagawa,<sup>1</sup> X. R. Zhou,<sup>2</sup> Toshio Suzuki,<sup>3</sup> and N. Yoshida<sup>4</sup><sup>1</sup>Center for Mathematics and Physics, University of Aizu, Aizu-Wakamatsu, Fukushima 965-8580, Japan<sup>2</sup>Department of Physics and Institute of Theoretical Physics and Astrophysics, Xiamen University, Xiamen 361005, People's Republic of China<sup>3</sup>Department of Physics, College of Humanities and Sciences, Nihon University, Sakurajosui 3-25-40, Setagaya-ku, Tokyo 156-8550, Japan<sup>4</sup>Faculty of Informatics, Kansai University, Takatsuki 569-1095, Japan

(Received 16 July 2008; revised manuscript received 26 August 2008; published 21 October 2008)

Magnetic dipole ( $M1$ ) transitions of  $N = 11$  nuclei  $^{17}\text{C}$  and  $^{21}\text{Ne}$  are investigated by using shell model and deformed Skyrme Hartree-Fock + blocked BCS wave functions. Shell model calculations predict well observed energy spectra and magnetic dipole transitions in  $^{21}\text{Ne}$ , while the results are rather poor to predict these observables in  $^{17}\text{C}$ . In the deformed HF calculations, the ground states of the two nuclei are shown to have large prolate deformations close to  $\beta_2 = 0.4$ . It is also pointed out that the first  $K^\pi = 1/2^+$  state in  $^{21}\text{Ne}$  is prolately deformed, while the first  $K^\pi = 1/2^+$  state in  $^{17}\text{C}$  is predicted to have a large oblate deformation close to the ground state in energy. We point out that the experimentally observed large hindrance of the  $M1$  transition between  $I^\pi = 1/2^+$  and  $3/2^+$  in  $^{17}\text{C}$  can be attributed to a shape coexistence near the ground state of  $^{17}\text{C}$ .

DOI: [10.1103/PhysRevC.78.041304](https://doi.org/10.1103/PhysRevC.78.041304)

PACS number(s): 23.20.Js, 21.60.Cs, 21.60.Jz, 27.20.+n

*I. Introduction.* Recently, many experimental and theoretical efforts have been made to study structure and reaction mechanisms in nuclei near drip lines. Electromagnetic observables can provide useful information for the study of the structure of nuclei, not only ground states but also excited states. These observables are expected to pin down precise information of the configuration and the deformation of nuclei. Advanced experimental instruments reveal several unexpected structures of light nuclei with the mass number  $A \sim 10$ – $20$ . One of the current issues is a large quenching of the magnetic dipole ( $M1$ ) transition between the first excited  $1/2^+$  state and the ground state with  $I^\pi = 3/2^+$  in  $^{17}\text{C}$  [1] in comparison with the corresponding transitions in one of the  $N = 11$  isotones,  $^{21}\text{Ne}$  [2].

The deformation manifests itself in observables like  $E2$  and  $M1$  moments. In Ref. [3], deformed Skyrme Hartree-Fock (HF) + BCS calculations were performed to study the evolution of deformations in C and Ne isotopes. The calculated electric quadrupole moments and magnetic moments were successfully compared with empirical data. It was pointed out that the shell occupancy gives the crucial effect on the evolution of the deformation of isotope chains. This deformation driving mechanism due to the shell occupancy has been noticed as the nuclear Jahn-Teller effect [4], which gives an intuitive understanding of the evolution of deformation. A possible shape coexistence is pointed out in  $^{17}\text{C}$  because of different deformation driving effects between neutrons and protons. Namely, the first excited  $K^\pi = 1/2^+$  state has oblate deformation and almost degenerates with the prolately deformed ground state with  $K^\pi = 3/2^+$ . On the other hand, there is no sign of shape coexistence in  $^{21}\text{Ne}$  because the shell occupancies are almost the same between protons and neutrons. From a theoretical point of view, it is interesting to see how many differences and similarities will appear between the results of standard shell model calculations and those of mean field theories. To this end, the HF results are compared with shell model results to investigate similarities and differences between the two models in observables

such as excitation energies and  $M1$  transitions in  $^{17}\text{C}$  and  $^{21}\text{Ne}$ .

In this article, we extend the previous calculations in Ref. [3] and particularly focus on recent experimental data of  $M1$  transitions in  $^{17}\text{C}$  and  $^{21}\text{Ne}$  to study possible shape coexistence near the ground states of  $^{17}\text{C}$ . This article is organized as follows. We study the energy levels, magnetic moments, and  $M1$  transitions by using shell model wave functions in Sec. II. The deformed HF + blocked BCS results are shown in Sec. III. A summary is given in Sec. IV.

*II. Shell model calculations of  $^{17}\text{C}$  and  $^{21}\text{Ne}$ .* In light and medium mass nuclei, the shell model is one of the most successful theories to describe nuclear structure in both the ground states and the excited states. Shell model calculations are performed in (p-sd) model space for  $^{17}\text{C}$  and (sd) model space for  $^{21}\text{Ne}$  with three effective interactions PSDMK2 [5], SFO [6], and WBP [7]. The excitation energies of the first  $I^\pi = 3/2^+$ ,  $1/2^+$ , and  $5/2^+$  states are tabulated in Table I. The SFO interaction is identical to the PSDMK2 interaction in (sd) model space so that the two results are the same for  $^{21}\text{Ne}$ . The excitation energies of  $^{21}\text{Ne}$  are well reproduced by all three shell model calculations. It is not surprising because the effective force is usually fitted to the data of stable nuclei such as  $^{21}\text{Ne}$ . The results of WBP show the best agreement with experimental excitation energies within a 100 keV difference. The calculated results are much worse in the case of  $^{17}\text{C}$ . The interactions PSDMK2 and SFO predict the spin-parity of the ground state to be  $I^\pi = 1/2^+$ , while the observed spin-parity is  $I^\pi = 3/2^+$ . The interaction WBP gives a state with  $I^\pi = 3/2^+$  as the ground state. However,  $5/2^+$  is almost degenerate with the ground state contrary to the experimental data.

Magnetic moments and magnetic dipole ( $M1$ ) transition probabilities  $B(M1)$  are given in Tables II and III, respectively. The magnetic operator is defined as

$$\mu_{\text{eff}} = (g_s^{\text{bare}} + \delta g_s)\mathbf{s} + (g_l^{\text{bare}} + \delta g_l)\mathbf{l} + g_p[Y_s \times \mathbf{s}]^{(1)}, \quad (1)$$

where  $\delta g_s$  and  $\delta g_l$  are the renormalization factors for the spin and the orbital  $g$  factors, respectively. The last term of Eq. (1)

TABLE I. Shell model calculations of excitation energies in  $^{17}\text{C}$  and  $^{21}\text{Ne}$ . The shell model calculations were performed by using effective interactions PSDMK2, SFO, and WBP. For sd shell configurations, the interaction matrices of PSDMK2 and SFO are the same. Experimental data are taken from Ref. [1] for  $^{17}\text{C}$  and from Ref. [2] for  $^{21}\text{Ne}$ . All units are in MeV.

	Int.	$\frac{3}{2}^+$	$\frac{1}{2}^+$	$\frac{5}{2}^+$	$\frac{5}{2}^+$	$\frac{1}{2}^+$
$^{17}\text{C}$	MK2	0.305	0.0	0.711	1.679	5.007
	SFO	0.304	0.0	0.654	1.678	5.039
	WBP	0.0	0.295	0.032	1.998	5.034
	Exp	0.0	(0.212)	0.333		
	Int.	$\frac{3}{2}^+$	$\frac{1}{2}^+$	$\frac{5}{2}^+$	$\frac{5}{2}^+$	$\frac{1}{2}^+$
$^{21}\text{Ne}$	MK2 (SFO)	0.0	1.930	0.495	3.250	4.688
	WBP	0.0	2.870	0.249	3.484	5.815
	Exp	0.0	2.794	0.351	3.735	

is the tensor component due to the core polarization effect. The shell model results of magnetic moments are shown in Table II with the bare  $g$  factors and the effective  $g$  factors for the IV channels,  $\delta g_s = -0.2g_s^{\text{IV}}\tau_z = -0.2\frac{(g_s^{\text{IV}}-g_s^{\text{IV}})}{2}\tau_z$ ,  $\delta g_l = -0.15\tau_z$ , and  $g_p = -1.0\tau_z$ . For the magnetic moments, the effects of  $\delta g_s$  and  $\delta g_l$  cancel each other largely and that of the tensor component  $g_p$  is very small. The net effect of the effective operator is less than 5% in  $^{17}\text{C}$  and 20% in  $^{21}\text{Ne}$ . In comparison with experimental data, the optimum quenching factor  $\delta g_s$  depends on the model space and the effective interaction. For  $^{17}\text{C}$ , small quenching factors ( $\delta g_s/g_s^{\text{IV}} \sim 0.0$  for PSDMK2 and SFO,  $\delta g_s/g_s^{\text{IV}} \sim -0.2\tau_z$  for WBP) give good agreement with the experimental data. Slightly larger values ( $\delta g_s/g_s^{\text{IV}} \sim -0.25\tau_z$  for PSDMK2 and SFO,  $\delta g_s/g_s^{\text{IV}} \sim -0.2\tau_z$  for WBP) give reasonable results in the case of  $^{21}\text{Ne}$ .

In Table III, two empirical  $M1$  transition probabilities in  $^{21}\text{Ne}$  are reasonably well reproduced by the shell model calculations. The best results among the three interactions are given by the WBP interaction with the effective spin  $g$  factor  $\delta g_s/g_s^{\text{IV}} = -0.2\tau_z$ . We can see in Tables I, II, and III that the shell model provides good agreement not only for

TABLE III. Shell model  $B(M1)$  in  $^{17}\text{C}$  and  $^{21}\text{Ne}$  in units of  $\mu_N^2$  with the bare  $g$  factors (the effective  $g$  factors). Experimental data are taken from Ref. [1] for  $^{17}\text{C}$  and Ref. [2] for  $^{21}\text{Ne}$ . See the caption to Table II for details.

	Int.	$\frac{1}{2}^+ \rightarrow \frac{3}{2}^+$	$\frac{5}{2}^+ \rightarrow \frac{3}{2}^+$
$^{17}\text{C}$	MK2	0.084(0.045)	0.070(0.031)
	SFO	0.077(0.041)	0.077(0.035)
	WBP	0.078(0.043)	0.077(0.034)
	Exp	$0.010 \pm 0.001$	$0.082 + 0.032/-0.018$
	Int.	$\frac{1}{2}^+ \rightarrow \frac{3}{2}^+$	$\frac{5}{2}^+ \rightarrow \frac{3}{2}^+$
$^{21}\text{Ne}$	MK2	0.724(0.607)	0.173(0.128)
	WBP	0.451(0.390)	0.161(0.109)
	Exp	$0.33 \pm 0.05$	$0.128 \pm 0.03$

the excitation energies but also for the magnetic moments and  $M1$  transition probabilities in  $^{21}\text{Ne}$ . In  $^{17}\text{C}$ , the  $M1$  transition probability from  $I^\pi = 5/2^+$  to  $3/2^+$  is reproduced well by the shell model with the bare  $g$  factors. However, the transition probability from  $I^\pi = 1/2^+$  to  $3/2^+$  is very poorly predicted; i.e., the empirical data are almost one order of magnitude smaller than the shell model predictions with the bare  $g$  factors. The effective  $g$  factors adopted in the magnetic moments in Table II decrease substantially the  $B(M1)$  values in  $^{17}\text{C}$ . However, these effective  $g$  factors do not give any satisfactory results for the measured two transitions between  $I^\pi = 5/2^+ \rightarrow 3/2^+$  and  $I^\pi = 1/2^+ \rightarrow 3/2^+$  as shown in parentheses in Table III. Recently, the description of  $M1$  transitions in  $^{17}\text{C}$  has been considerably improved with the use of a modified SFO Hamiltonian [10].

III. *Deformations and magnetic dipole transitions in  $^{17}\text{C}$  and  $^{21}\text{Ne}$ .* The neutron number dependence of deformations was studied along the chain of C and Ne isotopes in Ref. [3] by performing deformed HF + blocked BCS calculations with Skyrme interactions SGII and SIII. In this study, we perform the same deformed HF calculations of two  $N = 11$  isotones  $^{17}\text{C}$  and  $^{21}\text{Ne}$  with a different Skyrme interaction SkO'. We found that the results of SkO' are very close to those of SGII

TABLE II. Magnetic moments in  $^{17}\text{C}$  and  $^{21}\text{Ne}$  in units of  $\mu_N^2$ . The shell model calculations were performed by using effective interactions PSDMK2, SFO, and WBP with the bare  $g$  factors. The values in parentheses for  $\frac{3}{2}^+$  in  $^{17}\text{C}$  and  $\frac{3}{2}^+$  and  $\frac{5}{2}^+$  for  $^{21}\text{Ne}$  were obtained by using the effective  $g$  factors for the IV channels,  $\delta g_s = -0.2g_s^{\text{IV}}\tau_z$ ,  $\delta g_l = -0.15\tau_z$ , and  $g_p = -1.0\tau_z$  in Eq. (1). Experimental data of magnetic moments are taken from Ref. [8] for  $^{17}\text{C}$  and from Ref. [9] for  $^{21}\text{Ne}$ .

$^{17}\text{C}$	$\frac{3}{2}^+$	$\frac{1}{2}^+$	$\frac{5}{2}^+$	$\frac{5}{2}^+$	$\frac{1}{2}^+$
MK2	-0.710(-0.686)	-1.548	-1.453	-1.447	0.280
SFO	-0.725(-0.713)	-1.548	-1.500	-1.424	0.232
WBP	-0.858(-0.819)	-1.566	-1.404	-1.744	0.570
Exp	0.758(38)				
$^{21}\text{Ne}$	$\frac{3}{2}^+$	$\frac{1}{2}^+$	$\frac{5}{2}^+$	$\frac{5}{2}^+$	$\frac{1}{2}^+$
MK2	-0.887(-0.720)	-1.498	-0.657(-0.484)	-0.403	0.228
WBP	-0.824(-0.674)	-1.548	-0.643(-0.518)	-0.692	0.127
Exp	-0.661797(5)  0.49(4) ,  0.70(8) ,  0.88(20)				

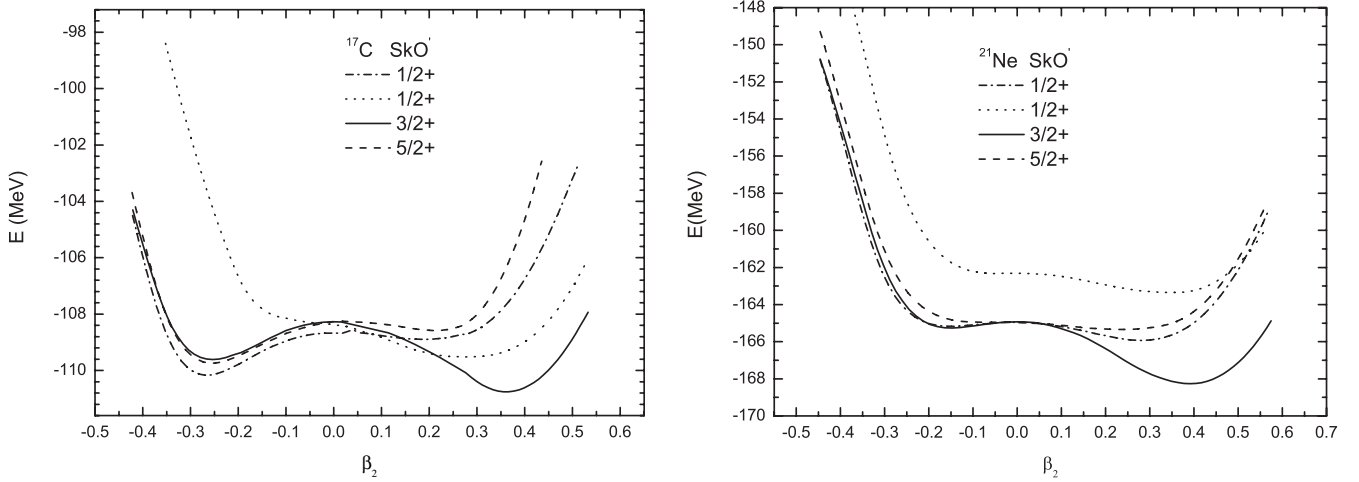


FIG. 1. Energy surfaces as a function of deformation parameter  $\beta_2$  in  $^{17}\text{C}$  and  $^{21}\text{Ne}$ . Deformed HF + blocked BCS calculations are performed with the Skyrme interaction SkO'.

and SIII. One advantage of SkO' is to give an oblate deformed ground state for  $^{12}\text{C}$  with the original spin-orbit interaction, while the spin-orbit interaction was reduced in SIII and SGII to obtain the oblate deformation. In numerical calculations, the axial symmetry is assumed for the HF deformed potential. The pairing interaction is taken to be a density dependent pairing interaction in BCS approximation. For numerical details about the pairing calculations, see Refs. [11] and [12].

Deformed Skyrme HF + blocked BCS results are shown in Fig. 1(a) for  $^{17}\text{C}$  and Fig. 1(b) for  $^{21}\text{Ne}$ . The deformation and the intrinsic  $Q_0$  moments are tabulated in Table IV for  $^{17}\text{C}$  and  $^{21}\text{Ne}$ . The ground states are predicted to be the  $K^\pi = 3/2^+$  state in both nuclei having large prolate deformations  $\beta_2 = 0.366$  for  $^{17}\text{C}$  and  $0.391$  for  $^{21}\text{Ne}$ . The spin-parity of calculated results can be compared with the observed ones  $I^\pi = 3/2^+$  in both nuclei. In  $^{17}\text{C}$ , the first excited state is predicted to be the  $K^\pi = 1/2^+$  state with a large oblate deformation  $\beta_2 = -0.270$ . The energy difference from the ground state is rather small with  $E_x = 0.56$  MeV. On the other hand, the first excited  $K^\pi = 1/2^+$  in  $^{21}\text{Ne}$  is predicted to have a large

prolate deformation  $\beta_2 = 0.287$  with a large excitation energy  $E_x = 2.33$  MeV. This difference in the  $K^\pi = 1/2^+$  state can be understood as a manifestation of the nuclear Jahn-Teller effect due to the proton configuration [4]. In general, a few particles top of the closed shell drive prolate deformation, while a few holes prefer oblate deformation. There is strong competition between prolate driving  $N = 11$  neutrons and oblate driving  $Z = 6$  protons in  $^{17}\text{C}$ . Namely, the  $Z = 6$  proton configuration, two proton holes in the  $Z = 8$  closed shell, prefers the oblate deformation as is the case for the ground state of  $^{12}\text{C}$ , while the  $N = 11$  neutrons tend to drive prolate deformation. Consequently, in  $^{17}\text{C}$ , the ground state is prolately deformed due to the effect of neutron configuration. However, the first excited  $K^\pi = 1/2^+$  state becomes oblate under the influence of the deformation driving force of protons. In  $^{21}\text{Ne}$ , both the proton and neutron configurations drive prolate deformation so that there is no sign of the shape coexistence. The observed excitation energy of the first  $I^\pi = 1/2^+$  state is very low in  $^{17}\text{C}$  as  $E_x = 0.212$  MeV, while that of  $^{21}\text{Ne}$  is higher as  $E_x = 2.79$  MeV. These experimental observations

TABLE IV. Energies, deformations,  $Q$  moments, and magnetic moments in  $^{17}\text{C}$  and  $^{21}\text{Ne}$  with the Skyrme interaction SkO'. The magnetic moment  $\mu$  is calculated for the  $I = K$  state with the bare neutron  $g$  factor. Experimental data are the same as those for Table II (experimental uncertainties are omitted).

	$K^\pi$	$E_x$	$\beta_2$	$Q_{0p}$ (fm <sup>2</sup> )	$Q_{0n}$ (fm <sup>2</sup> )	$g_k$	$\mu$ ( $\mu_N$ )	$\mu(\text{exp})$ ( $\mu_N$ )
$^{17}\text{C}$	$\frac{3}{21}^+$	0.0	0.366	16.24	53.05	-1.197	-0.877	0.758
	$\frac{1}{21}^+$	0.56	-0.270	-15.27	-35.94	-3.420	-1.767	
	$\frac{5}{21}^+$	0.99	-0.247	-13.40	-34.43	-0.764	-1.126	
	$\frac{1}{22}^+$	1.21	0.272	13.59	40.75	-1.101	-0.947	
	$^{21}\text{Ne}$	$\frac{3}{21}^+$	0.0	0.391	42.15	46.98	-1.112	-0.728
	$\frac{1}{21}^+$	2.33	0.287	31.67	32.05	-2.557	-1.523	
	$\frac{5}{21}^+$	2.92	0.226	25.85	23.83	-0.764	-1.040	0.49  ~  0.88
	$\frac{1}{22}^+$	4.91	0.357	39.570	43.547	-0.231	-0.594	

are consistent with the calculated results in Table IV as far as the excitation energies are concerned. Thus we identify the first excited  $I^\pi = 1/2^+$  state as  $K^\pi = 1/2^+$  in both  $^{17}\text{C}$  and  $^{21}\text{Ne}$  with different large deformations  $\beta_2 = -0.270$  and  $0.287$ , respectively. The  $I = 1/2^+$  in  $^{21}\text{Ne}$  was interpreted in Ref. [13] as the head of rotational band with a large prolate deformation [13]. The  $I^\pi = 5/2^+$  state is observed at very low excitation energy around  $E_x = 0.3$  MeV in both nuclei. In the HF calculations, no  $K^\pi = 5/2^+$  state appears at the energy below  $E_x \sim 1$  MeV. Thus, we interpret that the observed first excited  $I^\pi = 5/2^+$  state in both nuclei is a member of the rotational band with  $K^\pi = 3/2^+$ . In the case of  $^{21}\text{Ne}$ , the ground state and the first excited state were identified as members of the same rotational band giving consistent predictions for the associated observed properties [14]. This interpretation is also supported by the large deformation length observed in the excitation to  $I^\pi = 5/2^+$  state in the proton inelastic scattering on  $^{17}\text{C}$  [15].

We study the magnetic dipole transitions between the excited and ground states in  $^{17}\text{C}$  and  $^{21}\text{Ne}$  using the deformed HF wave functions.

For axially symmetric deformation, the deformed many-particle initial and final states are expressed as a direct product of neutron and proton single-particle states;

$$|K\rangle = |\nu\rangle|\pi\rangle, \quad (2)$$

where the component of the total angular momentum along the symmetry axis is denoted by  $K$  [16,17] and  $|\nu(\pi)\rangle = a_{\rho_1}^\dagger a_{\rho_2}^\dagger \cdots |f(\beta_2)\rangle$  denotes the multi-quasiparticle neutron (proton) state. The state  $|f(\beta_2)\rangle$  is the quasiparticle vacuum with deformation  $\beta_2$ . The quasiparticle operator  $a^\dagger$  is connected to the real particle operators  $c^\dagger(\beta_2)$  and  $c(\beta_2)$  in the deformed basis by

$$a_{\lambda\mu}^\dagger(\beta_2) = u_{\lambda\mu}(\beta_2)c_{\lambda\mu}^\dagger(\beta_2) - v_{\lambda\mu}(\beta_2)c_{\lambda\mu}(\beta_2), \quad (3)$$

where  $\lambda$  specifies the quantum numbers of Nilsson orbit,  $v_{\lambda\mu}(\beta_2)$  is the BCS occupation amplitude, and  $u_{\lambda\mu}(\beta_2) = \sqrt{1 - v_{\lambda\mu}(\beta_2)^2}$ . The operators  $c_{\lambda\mu}^\dagger(\beta_2)$  and  $c_{\lambda\mu}(\beta_2)$  are further expanded by the spherical bases as  $c_{\lambda\mu}^\dagger(\beta_2) = \sum_a d_{\lambda a}^\mu(\beta_2)c_{a\mu}^\dagger$ , where the amplitude  $d_{\lambda a}^\mu(\beta_2)$  is denoted by the quantum numbers  $a = (n, l, j)$ .

The intrinsic  $M1$  single-particle transition operator is expressed as

$$\mathcal{M}(M1) = \sqrt{\frac{3}{4\pi}}\mu_N \times \left( \sum_i ((g_l(i) - g_R)\mathbf{l}_i + (g_s(i) - g_R)\mathbf{s}_i) + g_R\mathbf{I} \right), \quad (4)$$

where  $g_l(i)$ ,  $g_s(i)$ , and  $g_R$  are the orbital, spin  $g$  factor, and gyromagnetic ratio of the rotor, respectively, in units of the nuclear magneton  $\mu_N = e\hbar/2m_p c$ .

The transition matrix element can be written for one neutron quasiparticle states as

$$\begin{aligned} & \langle \nu'\pi'K' | \mathcal{M}(M1) | \nu\pi K \rangle \\ & = \langle \nu' | a_{\lambda'K'}(\beta_2) \mathcal{M}(M1) a_{\lambda K}^\dagger(\beta_2) | \nu \rangle \langle \pi' | \pi \rangle, \end{aligned} \quad (5)$$

where  $\langle \pi' | \pi \rangle$  and  $\langle \nu' | \nu \rangle$  are quasi-particle vacuum overlaps of neutrons and protons, respectively.

The in-band  $M1$  transition probability can be written, for a band with  $K > \frac{1}{2}$ , as

$$\begin{aligned} & B(M1; K I_1 \rightarrow K, I_2 = I_1 \pm 1) \\ & = \frac{3}{4\pi} \mu_N^2 (g_K - g_R)^2 K^2 \langle I_1 K 10 | I_2 K \rangle^2, \end{aligned} \quad (6)$$

where  $g_R = \frac{Z}{A}$  and  $g_K$  is the intrinsic  $g$  factor,  $K g_K = \langle K | g_l l_3 + g_s s_3 | K \rangle$ . The magnetic moment is expressed as

$$\mu = g_R I + (g_K - g_R) \frac{K^2}{I + 1}. \quad (7)$$

For the  $K \neq K'$  case, the  $M1$  transition probability is written to be

$$\begin{aligned} & B(M1; K I_1 \rightarrow K', I_2) \\ & = \frac{3}{4\pi} \mu_N^2 \times \langle I_1 K 1 K' - K | I_2 K' \rangle^2 G^2 \langle \pi' | \pi \rangle^2, \end{aligned} \quad (8)$$

where

$$\begin{aligned} G & = (g_s - g_R) \langle \nu' | a_{\lambda'K'}(\beta_2) s_{\Delta K} a_{\lambda K}^\dagger(\beta_2) | \nu \rangle \\ & + (g_l - g_R) \langle \nu' | a_{\lambda'K'}(\beta_2) l_{\Delta K} a_{\lambda K}^\dagger(\beta_2) | \nu \rangle, \end{aligned} \quad (9)$$

with  $\Delta K = K' - K$ .

The calculated  $B(M1)$  values are tabulated in Table V. We adopt  $g_s^{\text{eff}} = 0.5g_s^{\text{bare}}$  and  $g_s^{\text{eff}} = 0.7g_s^{\text{bare}}$  for the effective neutron spin  $g$  factor in the calculations. One can see a large hindrance in  $B(M1)$  from the  $I_1 = 1/2^+$  to  $I_1 = 3/2^+$  transition in  $^{17}\text{C}$ . This is entirely due to the shape difference between the ground and the first excited states. Namely, the value of the core overlap of BCS vacuums  $\langle q' | q \rangle \equiv \langle \nu' | \nu \rangle \langle \pi' | \pi \rangle$  is calculated to be  $\langle q'(\beta_2 = 0.366) | q(\beta_2 = -0.270) \rangle = 0.0378$  between  $I = 3/2_1^+$  and  $I = 1/2_1^+$  states in  $^{17}\text{C}$ . On the other hand the corresponding overlap in  $^{21}\text{Ne}$  is close to 1.0, i.e.,  $\langle q'(\beta_2 = 0.391) | q(\beta_2 = 0.287) \rangle = 0.982$  because both the initial and the final state have large prolate deformations. For the in-band transition ( $I_1 = 5/2^+ \rightarrow I_2 = 3/2^+$ ,  $K = 3/2$ ), the calculated  $B(M1)$  values with the  $g$  factor  $g_s^{\text{eff}} = 0.5g_s^{\text{bare}}$  agree well with the observed ones within the experimental accuracies. This quenching factor is somewhat smaller than the adopted values in rare-earth nuclei, but it is still in the acceptable range. The  $g$  factor  $g_s^{\text{eff}} = 0.7g_s^{\text{bare}}$  gives better results for the transition ( $I_1 = K_1 = 1/2^+ \rightarrow I_2 = K_2 = 3/2^+$ ) in  $^{21}\text{Ne}$ . The deformed HF calculations gives the lowest  $K_1^\pi = 1/2^+$  state having asymptotic quantum numbers

TABLE V.  $M1$  transition probabilities  $B(M1)$  in  $^{17}\text{C}$  and  $^{21}\text{Ne}$  in units of  $\mu_N^2$ . The deformed HF calculations are performed by using the Skyrme interaction SkO'. The effective spin  $g$  factor  $g_s^{\text{eff}} = 0.5g_s^{\text{bare}}$  ( $0.7g_s^{\text{bare}}$ ) is adopted. Experimental data are taken from Ref. [1] for  $^{17}\text{C}$  and from Ref. [2] for  $^{21}\text{Ne}$ .

	$I_1(K) = \frac{1}{2}_1^+ \rightarrow I_2(K') = \frac{3}{2}_1^+$	$K = \frac{3}{2}, I_1 = \frac{5}{2}_1^+ \rightarrow I_2 = \frac{3}{2}_1^+$
$^{17}\text{C}$	0.00068(0.00094)	0.116(0.179)
exp	$0.010 \pm 0.001$	$0.082 + 0.032 - 0.018$
$^{21}\text{Ne}$	0.208(0.272)	0.152(0.224)
exp	$0.33 \pm 0.05$	$0.128 \pm 0.003$



$[Nn_3\Lambda\Omega] = [2201/2]$ . There is another  $K^\pi = 1/2^+$  state with  $[Nn_3\Lambda\Omega] = [2111/2]$  having slightly higher energy. The latter has a  $B(M1)$  value about two times larger for the transition to the  $K = 3/2$  ground state. It is expected that a small mixing of the  $[Nn_3\Lambda\Omega] = [2111/2]$  state increases the  $B(M1)$  value between the ( $I_1 = K_1 = 1/2^+ \rightarrow I_2 = K_2 = 3/2^+$ ). We notice that the optimal quenching spin  $g$  factor of the deformed HF results is slightly smaller than that of the shell model calculations. It is an interesting open question to compare more systematically the transition strength of two models at a quantitative level. It was mentioned in Ref. [1] that the halo effect of  $^{17}\text{C}$  may play a role in decreasing the  $B(M1)$  value of ( $I_1 = 1/2^+ \rightarrow I_2 = 3/2^+$ ). However no serious attempt has been made so far to take into account the halo effect on the  $M1$  transitions in  $^{17}\text{C}$ .

The calculated magnetic moments  $\mu$  are shown in Table IV. The observed magnetic moments show a small quenching effect in comparison with the calculated values for the ground states of  $^{17}\text{C}$  and  $^{21}\text{Ne}$ . The results of deformed HF calculations provide quantitative predictions similar to those of the shell models as far as the magnetic moments of the ground states are concerned. The observed magnetic moment for the excited  $I^\pi = 5/2^+$  state in  $^{21}\text{Ne}$  is still not accurate enough to perform precise comparison with the calculated results.

The second  $K = 1/2^+$  state is found in Table IV at rather low energy  $E_x = 1.21$  MeV  $^{17}\text{C}$  by the deformed HF model, while the  $I = 1/2_2^+$  state is located at  $E_x \sim 5$  MeV in the shell model calculations in Table I. So far the second  $1/2^+$  is not identified experimentally [18]. It is quite interesting to find the  $1/2_2^+$  state experimentally to disentangle the applicability of the two models.

*IV. Summary.* We have studied the magnetic dipole transitions in  $^{17}\text{C}$  and  $^{21}\text{Ne}$  using microscopic shell model wave functions and deformed HF wave functions. The energy

spectra as well as  $M1$  transition probabilities of  $^{21}\text{Ne}$  are well reproduced by the shell model calculations, while we need a quenching factor for the spin  $g$  factor to obtain reasonable quantitative agreement. On the other hand, the observed  $M1$  transition probability from the first excited  $1/2^+$  to the  $3/2^+$  ground state in  $^{17}\text{C}$  was found to be hindered by one order of magnitude compared with the shell model calculations. The shell model prediction of energy spectra is also poor in  $^{17}\text{C}$  compared with the experimental data. The deformed HF + blocked BCS calculations are performed with the Skyrme interaction SkO'. The ground states of  $^{17}\text{C}$  and  $^{21}\text{Ne}$  are predicted as largely prolate deformed states with  $K^\pi = 3/2^+$ . In  $^{21}\text{Ne}$ , the first  $K^\pi = 1/2^+$  state appears at the energy  $E_x \sim 2.3$  MeV with a large prolate deformation. On the other hand, the first  $K^\pi = 1/2^+$  state in  $^{17}\text{C}$  has a large oblate deformation with  $E_x \sim 0.5$  MeV as the result of competition between the deformation driving force of protons and neutrons. The calculated energy difference between  $K^\pi = 3/2^+$  and  $K^\pi = 1/2^+$  states is close to the observed energy difference between  $I^\pi = 3/2^+$  and  $I^\pi = 1/2^+$  states in both  $^{21}\text{Ne}$  and  $^{17}\text{C}$ . The strong hindrance of the  $B(M1)$  transition between the first excited  $1/2^+$  to the ground state  $3/2^+$  of  $^{17}\text{C}$  can be attributed to the shape difference between the lowest  $K^\pi = 1/2^+$  and the first  $K^\pi = 3/2^+$  state as is predicted by the deformed HF + blocked BCS calculations.

We thank H. Sakurai for communications on experimental data prior to publication. This work is supported in part by the Japanese Ministry of Education, Culture, Sports, Science and Technology by a Grant-in-Aid for Scientific Research under Program Numbers C(2)18540290 and 20540277, by the National Science Foundation of China under Contract 10605018, and by the Program for New Century Excellent Talents in University under Contract NCET-07-0730.

- 
- [1] D. Suzuki *et al.*, Phys. Lett. **B666**, 222 (2008).  
 [2] *Table of Isotopes*, edited by R. B. Firestone *et al.* (Wiley, New York, 1996).  
 [3] H. Sagawa, X. R. Zhou, X. Z. Zhang, and T. Suzuki, Phys. Rev. C **70**, 054316 (2004).  
 [4] H. A. Jahn and E. Teller, Proc. R. Soc. London, Ser. A **161**, 220 (1937); P.-G. Reinhard and E. W. Otten, Nucl. Phys. **A420**, 173 (1984); W. Nazarewicz, Int. J. Mod. Phys. E **2**, 51 (1993); Nucl. Phys. **A574**, 27c (1994).  
 [5] D. J. Millener and D. Kurath, Nucl. Phys. **A255**, 315 (1975).  
 [6] T. Suzuki, R. Fujimoto, and T. Otsuka, Phys. Rev. C **67**, 044302 (2003).  
 [7] E. K. Warburton and B. A. Brown, Phys. Rev. C **46**, 923 (1992); OXBASH, the Oxford, Buenos-Aires, Michigan State, Shell Model Program, B. A. Brown *et al.*, MSU Cyclotron Laboratory Report No. 524, 1986.  
 [8] H. Ogawa *et al.*, Eur. Phys. J. **A13**, 81 (2002).  
 [9] P. Raghaven, At. Data Nucl. Data Tables **42**, 189 (1989).  
 [10] T. Suzuki and T. Otsuka, Proceedings of ISPUN07, Hoi An, Vietnam (2007), p. 318 (to be published).  
 [11] H. Sagawa, T. Suzuki, and K. Hagino, Nucl. Phys. **A722**, 183 (2003).  
 [12] M. Bender, K. Rutz, P.-G. Reinhard, and J. A. Maruhn, Eur. Phys. J. **A 8**, 59 (2000).  
 [13] C. Rolfs *et al.*, Nucl. Phys. **A189**, 641 (1972).  
 [14] C. Rolfs *et al.*, Nucl. Phys. **A167**, 449 (1971).  
 [15] Z. Elekes *et al.*, Phys. Lett. **B614**, 174 (2005).  
 [16] A. Bohr and B. R. Mottelson, *Nuclear Structure* (Benjamin, Elmsford, NY, 1975), Vol. 2.  
 [17] S. G. Nilsson, Mat. Fys. Medd. Dan. Vid. Selsk. **29**, No. 16 (1955).  
 [18] H. G. Bohlen *et al.*, Eur. Phys. J. A **31**, 279 (2007).